⌘ *Author's Choice*

THE JOURNAL OF BIOLOGICAL CHEMISTRY VOL. 286, NO. 26, pp. 23378–23387, July 1, 2011


# Differential Distribution, Clustering, and Lateral Diffusion of Subtypes of the Inositol 1,4,5-Trisphosphate Receptor*[S]

Received for publication, March 2, 2011, and in revised form, April 27, 2011 Published, JBC Papers in Press, May 5, 2011, DOI 10.1074/jbc.M111.236372

**Evangelia Pantazaka and Colin W. Taylor**[1]

*From the Department of Pharmacology, University of Cambridge, Cambridge CB2 1PD, United Kingdom*

**Regulation of inositol 1,4,5-trisphosphate ($IP_3$) receptors ($IP_3R$) by $IP_3$ and $Ca^{2+}$ allows them to initiate and regeneratively propagate intracellular $Ca^{2+}$ signals. The distribution and mobility of $IP_3R$ determines the spatial organization of these $Ca^{2+}$ signals. Until now, there has been no systematic comparison of the distribution and mobility of the three mammalian $IP_3R$ subtypes in a uniform background. We used confocal microscopy and fluorescence recovery after photobleaching to define these properties for each $IP_3R$ subtype expressed heterologously in COS-7 cells. $IP_3R1$ and $IP_3R3$ were uniformly distributed within the membranes of the endoplasmic reticulum (ER), but the distribution of $IP_3R2$ was punctate. The mobile fractions ($M_f = 84 \pm 2$ and $80 \pm 2\%$) and diffusion coefficients ($D = 0.018 \pm 0.001$ and $0.016 \pm 0.002$ $\mu m^2/s$) of $IP_3R1$ and $IP_3R3$ were similar. Other ER membrane proteins (ryanodine receptor type 1 and sarco/endoplasmic reticulum $Ca^{2+}$-ATPase type 1) and a luminal protein (enhanced GFP with a KDEL retrieval sequence) had similar mobile fractions, suggesting that $IP_3R1$ and $IP_3R3$ move freely within an ER that is largely, although not entirely, continuous. $IP_3R2$ was less mobile, but $IP_3R2$ mobility differed between perinuclear ($M_f = 47 \pm 4\%$ and $D = 0.004 \pm 0.001$ $\mu m^2/s$) and near-plasma membrane ($M_f = 64 \pm 6\%$ and $D = 0.013 \pm 0.004$ $\mu m^2/s$) regions, whereas $IP_3R3$ behaved similarly in both regions. We conclude that $IP_3R1$ and $IP_3R3$ diffuse freely within a largely continuous ER, but $IP_3R2$ is more heterogeneously distributed and less mobile, and its mobility differs between regions of the cell.**

Inositol 1,4,5-trisphosphate ($IP_3$)[2] receptors ($IP_3R$) are tetrameric intracellular $Ca^{2+}$ channels that are expressed in the membranes of the endoplasmic reticulum (ER) of almost all animal cells (1, 2). The intrinsic channel opens when the $IP_3R$ binds both $Ca^{2+}$ and $IP_3$, with $IP_3$ effectively tuning the sensitivity of the $IP_3R$ to $Ca^{2+}$ (3, 4). The interplay between $IP_3$ and the $Ca^{2+}$ released by $IP_3R$ allows active $IP_3R$ to recruit regeneratively the activity of nearby $IP_3R$. This $Ca^{2+}$-induced $Ca^{2+}$ release allows $Ca^{2+}$ signals to grow from tiny local events, arising from openings of single $IP_3R$, into larger events ("$Ca^{2+}$ puffs"), reflecting the coordinated opening of several clustered $IP_3R$, and ultimately into regenerative $Ca^{2+}$ waves that may invade the entire cell (5–7). This hierarchical recruitment of $IP_3R$ is an essential feature of the spatially organized $Ca^{2+}$ signals that substantially underpin the versatility of $Ca^{2+}$ as an intracellular messenger (8).

Regulation of $IP_3R$ by $Ca^{2+}$ is one feature that allows regenerative recruitment of $IP_3R$ activity, but the other is the spatial relationship between $IP_3R$. Only closely spaced $IP_3R$ are likely to be influenced by each others' activities because cytoplasmic $Ca^{2+}$ buffers effectively insulate more widely separated $IP_3R$ from each other. Persuasive evidence from analyses of both $Ca^{2+}$ signals (6, 7, 9) and $IP_3R$ distribution (10–13) in intact cells and from patch-clamp recording of $IP_3R$ in the nuclear envelope (14–17) has established that $IP_3R$ can assemble into clusters. The relationships between these observations, whether $IP_3R$ assemble into clusters only when stimulated (16–18), and whether the three $IP_3R$ subtypes differ in these behaviors are unresolved. An issue that has become contentious is whether functional $IP_3R$ are mobile. Our analyses of $IP_3R$ in the nuclear envelope suggest that $IP_3R$ are randomly distributed and rapidly assemble into clusters only when stimulated with $IP_3$ (16, 17). This suggestion is consistent with analyses of $IP_3R$ motility using fluorescence recovery after photobleaching (FRAP), which suggest that most $IP_3R$ are mobile (11, 19–23), but high-resolution analyses of the local $Ca^{2+}$ signals evoked by $IP_3$ suggest that these sparse events are repeatedly initiated at the same point (7, 18). This suggests either that the small fraction of the cellular complement of $IP_3R$ that generates these events is immobile or that mobile $IP_3R$ initiate events only when they visit specific regions of a cell. Further understanding of $IP_3R$ mobility within cells is required to resolve these issues. Here, we extend previous studies of $IP_3R$ mobility by using confocal microscopy and FRAP to examine, for the first time, the distribution and mobility of each $IP_3R$ subtype in a single cell type, COS-7 cells.

## EXPERIMENTAL PROCEDURES

*Constructs*—Rat $IP_3R1$ (GenBank™ accession number GQ233032) (24) lacking the S1 splice region (25), mouse $IP_3R2$ (accession number GU980658) (12), and rat $IP_3R3$ (accession number GQ233031) (26) were used. The EYFP-$IP_3R1$ plasmid was prepared as described (27, 28). The plasmid encoding EGFP-$IP_3R1$ was made from a previously described plasmid for ECFP-$IP_3R1$ (29) by exchanging ECFP for EGFP. In brief,

* This work was supported by Medical Research Council UK Grant G0700843 and Wellcome Trust Grant 085295.

[S] The on-line version of this article (available at http://www.jbc.org) contains supplemental Figs. S1–S7, Tables S1 and S2, and additional references.

⌘ *Author's Choice*—Final version full access.

[1] To whom correspondence should be addressed: Dept. of Pharmacology, University of Cambridge, Tennis Court Rd., Cambridge CB2 1PD, UK. E-mail: cwt1000@cam.ac.uk.

[2] The abbreviations used are: $IP_3$, inositol 1,4,5-trisphosphate; $IP_3R$, $IP_3$ receptor(s); ER, endoplasmic reticulum; FRAP, fluorescence recovery after photobleaching; EYFP, enhanced yellow fluorescent protein; EGFP, enhanced green fluorescent protein; ECFP, enhanced cyan fluorescent protein; RyR1, ryanodine receptor type 1; ROI, region(s) of interest.

pENTR-ECFP-$IP_3R1$ was digested with MluI and NheI to excise ECFP, which was then replaced with EGFP (similarly excised from pENTR-EGFP). The vector was recombined into the pcDNA3.2/DEST expression vector using Gateway LR Clonase enzyme mixture (Invitrogen). The EGFP-$IP_3R2$ plasmid was prepared from a previously described construct, pENTR-$IP_3R2$ (30). PCR was used to amplify an N-terminal fragment of $IP_3R2$ (bases 1–3297) using the following primers (5′–3′): forward (P1), AGCATGCGCGCATGTCTGACAAAATGTC-CAGCTTCCTCTACATT; and reverse (P2), TATCGCTC-GAGTAACTGCACCTGTTTAAAGGCCTG. This fragment was digested with BssHII and XhoI and cloned into pENTR-EGFP-$IP_3R1$ digested with MluI and XhoI. This replaced the entire $IP_3R1$ sequence with the first 3297 bases of the $IP_3R2$ sequence, resulting in pENTR-EGFP-Nterm$IP_3R2$. This construct and pENTR-$IP_3R2$ were each digested with HaeII, and the HaeII fragment from pENTR-$IP_3R2$ was replaced with the HaeII fragment from pENTR-EGFP-Nterm$IP_3R2$ to give pENTR-EGFP-$IP_3R2$. This vector was recombined into the pcDNA3.2/DEST expression vector. A similar approach was used to construct the FLAG-$IP_3R2$ plasmid. PCR was used to amplify an N-terminal fragment of $IP_3R2$ from pENTR-$IP_3R2$ using the following primers (5′–3′): forward (P3), GCGT-CGACGCCACCATGGACTACAAAGACGATGACGATAA-GATGTCTGACAAAATGT; and reverse primer P2 (described above). The fragment was digested with SalI and XhoI and cloned in pENTR-1A. The N-terminal fragment and pENTR-$IP_3R2$ were digested with HaeII. The HaeII fragment from pENTR-$IP_3R2$ was then replaced with the HaeII fragment of the N-terminal to generate pENTR-FLAG-$IP_3R2$. This vector was recombined into the pcDNA3.2/DEST expression vector. For ECFP-$IP_3R3$, the existing clone of pENTR-ECFP-$IP_3R1$ (29) was used. PCR was used to amplify an N-terminal fragment of $IP_3R3$ (bases 1–4600) using the following primers (5′–3′): forward (P4), TGCATACGCGTATGAATGAAATGTCCAG-CTTTCTTCACATC; and reverse (P5), CAAGGACACTCGA-GCAGCCGGGTGGTGGAC. The PCR product was digested with MluI and XhoI, and it was then used to replace the MluI-XhoI-excised fragment of pENTR-ECFP-$IP_3R1$ to give pENTR-ECFP-Nterm$IP_3R3$. pENTR-$IP_3R3$ was digested with MfeI and EcoRI, and the excised fragment was used to replace the MfeI-EcoRI fragment of the pENTR-ECFP-Nterm$IP_3R3$ vector to give pENTR-ECFP-$IP_3R3$. This vector was recombined into the pcDNA3.2/DEST expression vector. The EGFP-$IP_3R3$ construct was made from the ECFP-$IP_3R3$ plasmid. In brief, pENTR-ECFP-$IP_3R3$ was digested with MluI and NheI to excise ECFP, which was then replaced with EGFP. The coding sequences of all $IP_3R$ were confirmed by sequencing. The plasmid encoding rabbit SERCA1 (sarco/endoplasmic reticulum $Ca^{2+}$-ATPase type 1) C-terminally tagged with EGFP was provided and sequenced by Dr. Malcolm East (University of Southampton, Hampshire, United Kingdom) (31). The plasmid encoding the EGFP sequence flanked by an N-terminal preprolactin leader sequence and a C-terminal KDEL motif (EGFP-KDEL) was provided and sequenced by Dr. Peter Haggie (University of California, San Francisco) (32). The plasmid encoding EGFP-ryanodine receptor type 1 (RyR1) was prepared as described (33).

*Cell Culture and Transfection*—COS-7 cells were grown in minimal essential medium supplemented with 10% fetal bovine serum and 2 mM L-glutamine at 37 °C in 5% $CO_2$. Cells (80–90% confluent) were transfected using Lipofectamine 2000 (1 $\mu$l/1 $\mu$g of DNA) (28). For immunofluorescence, cells grown on 13-mm diameter coverslips were transfected with 1 $\mu$g of DNA. For subcellular fractionation and FRAP assays, cells grown in 6-well plates and 35-mm dishes with glass bases (Scientific Laboratory Supplies, Yorkshire, United Kingdom), respectively, were transfected with 2–4 $\mu$g of DNA. For cotransfection with plasmids for two $IP_3R$ subtypes, 0.5 $\mu$g of DNA of each plasmid was used. Cells were used 24 h after transfection.

*Confocal Microscopy*—Transfected cells on coverslips were fixed with 3.5% paraformaldehyde in PBS (137 mM NaCl, 2.7 mM KCl, 10 mM $Na_2HPO_4$, and 2 mM $KH_2PO_4$, pH 7.4) at pH 7.4 for 5–20 min at 20 °C, washed with PBS, permeabilized with Triton X-100 (0.1% in PBS) for 5–10 min at 20 °C, and blocked by incubation with BSA (5% in PBS) for 10 min at 20 °C (28). Similar results were obtained after fixation with methanol/acetone (1:1, v/v) for 10 min at −20 °C (supplemental Fig. S1). All immunostaining was performed in PBS with 5% BSA, with three washes between steps. Calreticulin was visualized by incubating first with a rabbit anti-calreticulin antiserum (1:100; Calbiochem) for 2.5 h at 20 °C and then with an Alexa Fluor 633-labeled goat anti-rabbit secondary antibody (1:500; Molecular Probes) for 1 h at 20 °C. To identify FLAG-$IP_3R2$, cells were incubated with a mouse anti-FLAG antibody (1:1000; Sigma) for 2 h at 37 °C and then with an Alexa Fluor 488-labeled goat anti-mouse secondary antibody. Endogenous and/or heterologously expressed $IP_3R2$ or $IP_3R3$ was identified using affinity-purified rabbit antiserum to $IP_3R2$ (1:100; kindly provided by Dr. David Yule, University of Rochester) (34) or a mouse anti-$IP_3R3$ monoclonal antibody (1:100; Transduction Laboratories). Incubation with the primary antibodies for 2 h at 37 °C was followed by incubation with an Alexa Fluor 555-labeled goat anti-rabbit (or anti-mouse) secondary antibody (1:500; Molecular Probes). Coverslips were washed three times with PBS and once with water and then mounted in ProLong mounting medium (Molecular Probes).

Imaging was performed with a ×63 1.4-numerical aperture oil-immersion objective using a Leica TCS SP2 AOBS confocal microscope. ECFP, EGFP, EYFP, Alexa Fluor 488, Alexa Fluor 555, and Alexa Flour 633 were excited with the 458-, 488-, 514-, 488-, 541-, and 633-nm lines, respectively. Signals were collected using emission filters with detection bands of 468–550 (for ECFP alone; 468–500 when imaged simultaneously with EYFP), 500–565 (for EGFP alone; 500–525 when imaged with Alexa Fluor 555), 520–600, 500–580, 550–650, and 640–750 nm, respectively. No bleed-through was observed in the paired labeling. Images were exported as tiff files and processed using Adobe Photoshop.

*Subcellular Fractionation and Western Blotting*—Cells were washed with PBS, scraped into ice-cold PBS with protease inhibitors (one tablet/10 ml; Roche Applied Science), and disrupted by 30 passages through a 25-gauge needle. The lysate was centrifuged at 30,000 × *g* for 30 min, and the supernatant (S1, cytosolic proteins) was collected. The pellet was resuspended in 0.1 M $Na_2CO_3$ at pH 11.5, incubated on ice for 45 min

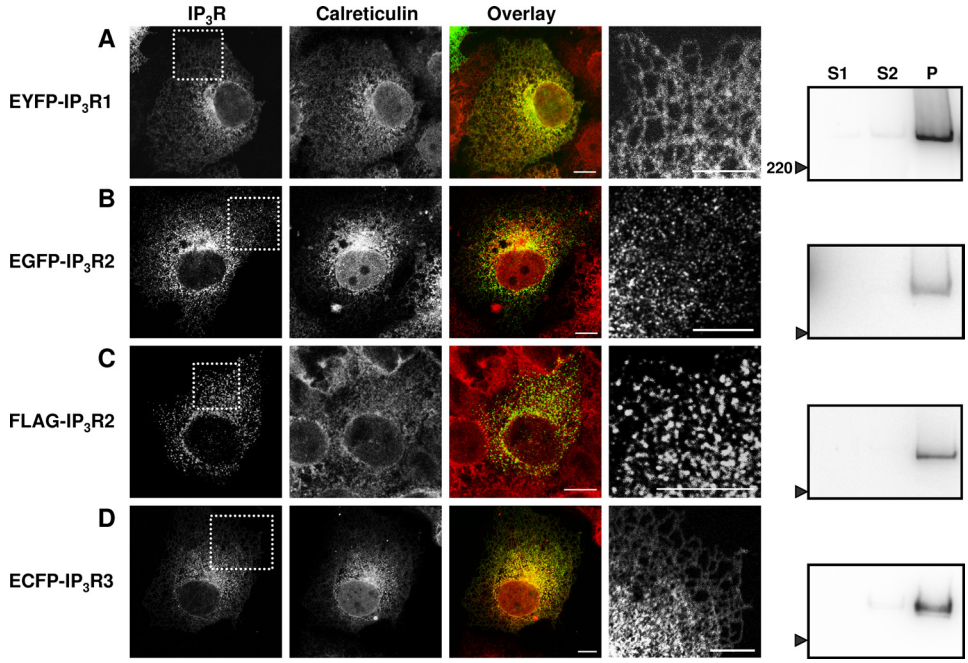


FIGURE 1. **Subcellular distribution of $IP_3R$ subtypes expressed in COS-7 cells.** *A–D*, typical confocal images of COS-7 cells expressing the indicated constructs. The *first* and *second columns* show the distribution of the expressed $IP_3R$ and of calreticulin, respectively. The *third column* shows overlays of the distribution of the two proteins ($IP_3R$ in *green* and calreticulin in *red*). The *fourth column* shows an enlargement of the *boxed areas* shown in the *first column*. Images are representative of three independent transfections. *Scale bars* = 10 $\mu$m. The *fifth column* shows Western blots probed with antibodies to GFP (*A* and *B*), FLAG (*C*), or $IP_3R3$ (*D*) after fractionation of the cells into S1 (cytosolic proteins), S2 (peripheral proteins), and P (pellet; integral membrane proteins) fractions. Each lane (*lanes S1*, *S2*, and *P*) was loaded with material derived from the same number of cells. The position of the 220-kDa molecular mass marker is shown. Each blot is representative of three independent transfections and fractionations.

to dissociate peripheral membrane proteins, and centrifuged at 30,000 × *g* for 30 min, and the second supernatant (S2, peripheral membrane proteins) was collected. The pellet (P, integral membrane proteins) was resuspended in PBS containing protease inhibitors and 1% Triton X-100 (28).

Samples (equivalent numbers of cells for each fraction) were loaded onto precast NuPAGE 3–8% Tris acetate gels (Invitrogen). SDS-PAGE, transfer (Invitrogen), and blotting were performed as described previously (28). Membranes were blocked by incubation in PBS containing 0.1% Tween (PBS-T) and 1% BSA for ~12 h and then incubated with primary antibody for 1 h in PBS-T with 1% BSA. Rabbit anti-GFP (1:1000; Abcam), mouse anti-FLAG (1:1000; Sigma) and mouse anti-$IP_3R3$ (1:1000) antibodies were used as primary antibodies. The membranes were then washed with PBS-T and incubated with a donkey anti-rabbit (1:2000) or goat anti-mouse (1:1000) secondary antibody (Santa Cruz Biotechnology) coupled to horseradish peroxidase for 1 h in PBS-T containing 1% BSA. The anti-FLAG antibody was itself preconjugated to peroxidase. Bands were detected using SuperSignal West Pico chemiluminescent substrate (Pierce).

*FRAP*—FRAP experiments were performed at 20 °C in culture medium supplemented with 20 mM Hepes at pH 7.3 using a Leica TCS SP5 AOBS microscope fitted with a ×63 1.4-numerical aperture oil-immersion objective and a pinhole diameter set for 1 Airy unit. Cells were illuminated with the 488-nm argon laser line (Lasos CW, 100 milliwatts), and signals were collected at 500–565 nm. Photobleaching experiments were performed using the Leica FRAP application wizard. Typically, fluorescence was recorded at 800-ms intervals (90-ms intervals for EGFP-KDEL) from 10 frames at 2% laser power before bleaching a 2.5-$\mu$m diameter region of interest (ROI) for 0.8 s at 100% laser power. Post-bleach images were then collected at 800-ms intervals using 2% laser power for up to 1000 s (typically 300 s). ROI were chosen to entirely exclude the nucleus, immediate perinuclear area (1–2 $\mu$m from the nucleus), and the plasma membrane. Only ROI where at least 70% of the initial fluorescence was bleached were used for analysis. Across all the experiments reported here, bleaching caused fluorescence

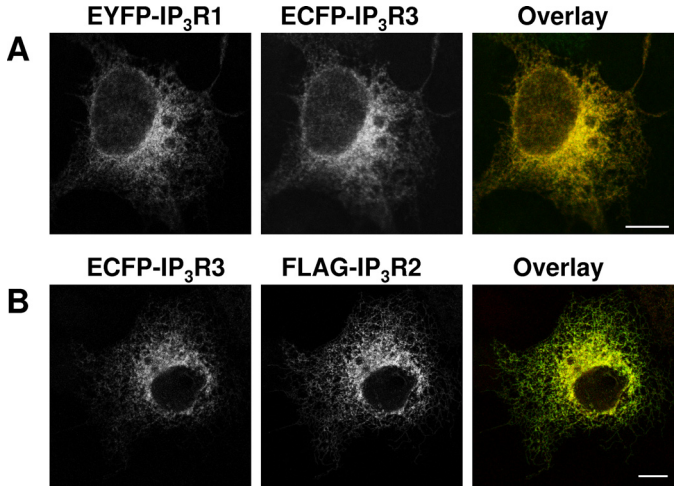


FIGURE 2. **Coexpression of pairs of $IP_3R$ subtypes results in a uniform reticular distribution.** *A* and *B*, COS-7 cells were transiently transfected with equal amounts of the indicated constructs. The *first* and *second columns* show the distribution of each $IP_3R$ subtype, and the *third column* shows the overlay (with the first construct in *green* and the second in *red*). *Scale bars* = 10 $\mu$m. Images are representative of three independent transfections.

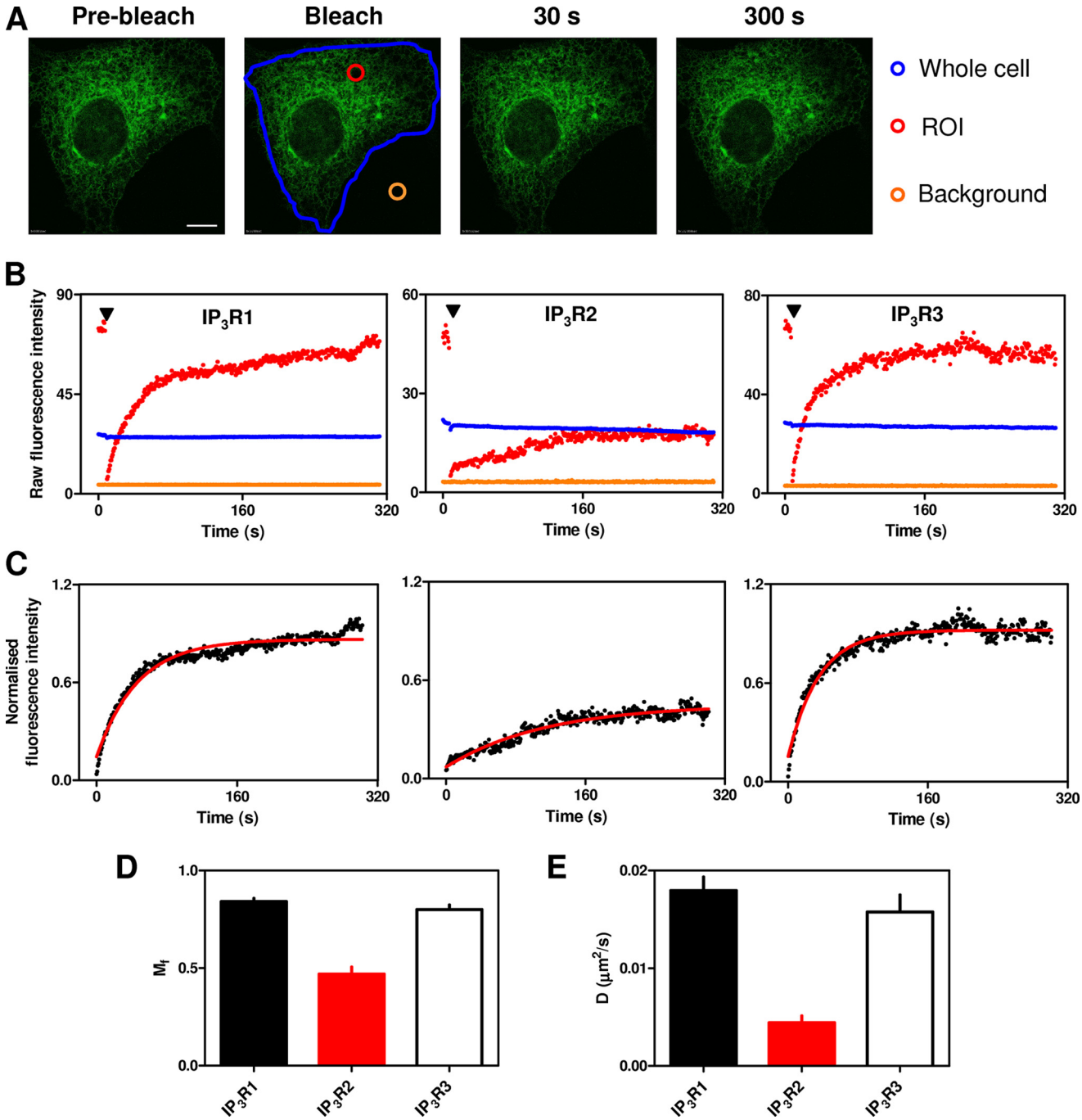


FIGURE 3. **Mobilities of $IP_3R$ subtypes.** *A*, a typical FRAP experiment is shown for EGFP-$IP_3R1$. Fluorescence was recorded from the entire cell (*blue outline*), the bleached ROI (*red circle*), and a background area outside the cell (*orange circle*). Typical images are shown before and after bleaching. *Scale bar* = 10 $\mu$m. *B*, raw fluorescence intensities are shown for the three regions color-coded as described for *A*. The *arrowheads* denote bleaching. *C*, normalized fluorescence intensities are shown after correction for background and loss of fluorescence with time. *Red lines* show the fitted monoexponential recovery curves (see "Experimental Procedures"). $M_f$ (*D*) and *D* (*E*) are shown for each $IP_3R$ subtype. The results in *D* and *E* are means ± S.E. from 23–30 cells. Supplemental Fig. S5 provides a comparison of the same data analyzed using another commonly used equation to describe the recovery phase.

within the ROI to decrease as follows: $IP_3R1$, 86 ± 2%; $IP_3R2$, 89 ± 1%; $IP_3R3$, 92 ± 1%; RyR1, 80 ± 4%; SERCA, 86 ± 2%; and EGFP-KDEL, 81 ± 1%.

*Analysis*—For every experiment, three reference regions were selected: the bleached ROI, a background region from outside the cell, and the whole cell (see Fig. 3*A*). All images were first corrected by subtracting background fluorescence. The average pixel intensity within the background area was subtracted from every pixel within the cell (ROI and whole cell); the corrected values were used for all subsequent analyses. Loss of fluorescence due to both image acquisition and bleaching of the ROI causes the whole cell fluorescence to decline with time. We corrected for this loss of fluorescence, which varied between both experiments and constructs ($IP_3R1$, 6 ± 1%; $IP_3R2$, 22 ± 4%; $IP_3R3$, 7 ± 1%; RyR1, 35 ± 3%; SERCA, 4 ± 1%; and EGFP-KDEL, 6 ± 1%), by expressing the fluorescence recorded from the ROI at each time as a fraction of that recorded from the whole cell at the same time. For convenience, all FRAP records

were also normalized by expressing this corrected fluorescence from the ROI as a fraction of its pre-bleach value (35). The half-time for recovery ($t_{½} = \ln 2/k$) was calculated by nonlinear curve fitting of the fluorescence recovery to a single exponential association equation (GraphPad Prism Version 5): $F_t = F_0 + (F_{max} - F_0)(1 - e^{-kt})$, where $F_t$ is the corrected fluorescence recorded from the ROI at time $t$; $F_0$ and $F_{max}$ are the fluorescence values obtained by extrapolation to immediately after the bleach and at infinite time after recovery, respectively; and $k$ is the first-order rate constant for recovery. The mobile fraction ($M_f$) was calculated from $(F_{max} - F_0)/(1 - F_0)$. Diffusion coefficients ($D$) were calculated from a two-dimensional diffusion equation: $D = (r^2\gamma)/(4t_{½})$, where $r$ is the radius of the ROI (1.25 $\mu$m), and $\gamma$ is a correction factor for bleaching (~1 for a circular beam) (36). Statistics were computed using Student's $t$ test or one-way analysis of variance (Bonferroni comparison test, 95% confidence intervals) as appropriate. All results are expressed as means ± S.E.

## RESULTS AND DISCUSSION

*Differential Subcellular Distributions of $IP_3R$ Subtypes*—After transient expression in COS-7 cells, EYFP-$IP_3R1$ (or EGFP-$IP_3R1$; data not shown) and ECFP-$IP_3R3$ (or EGFP-$IP_3R3$; data not shown) were uniformly localized to the ER. Each was distributed with a characteristic reticular pattern, and each colocalized with calreticulin, a luminal ER protein (Fig. 1, *A* and *D*). After crude fractionation, most $IP_3R$ were detected in the pellet (see "Experimental Procedures"). Western blot analysis with antiserum to GFP or $IP_3R3$ revealed single bands with the sizes expected for single subunits of $IP_3R1$ (~340 kDa) and $IP_3R3$ (~330 kDa) (Fig. 1, *A* and *D*, *fifth column*). These results confirm previous analyses of $IP_3R1$ (27, 28, 37–39) and $IP_3R3$ (19, 26, 39) distribution in COS cells using both immunocytochemistry of endogenous $IP_3R$ (26, 37) and expression of tagged $IP_3R$ (19, 27, 28, 38, 39).

The distribution of EGFP-$IP_3R2$ (Fig. 1*B*) was different from that of $IP_3R1$ and $IP_3R3$. Rather than uniformly populating the reticular ER, the distribution of EGFP-$IP_3R2$ was punctate, with the puncta apparently overlying the ER. Similar results were obtained with FLAG-$IP_3R2$ visualized using an anti-FLAG antibody (Fig. 1*C*), with EGFP-$IP_3R2$ and a different fixative (supplemental Fig. S1*A*), with endogenous $IP_3R2$ (see Fig. 4*E*), and with live cell imaging of EGFP-$IP_3R2$ (supplemental Fig. S1*B*). Others have also reported punctate distributions of native $IP_3R2$ (40) and heterologously expressed $IP_3R2$ (12), although in one study of COS-1 cells, there was no discernible difference between the distributions of $IP_3R1$ and $IP_3R2$ (38). $IP_3R2$ tagged with either EGFP or FLAG were recovered in the pellet fraction after subcellular fractionation (Fig. 1, *B* and *C*, *fifth column*), and each had the size expected (~335 and ~310 kDa, respectively). Enlarged images of the subcellular distribution of the three $IP_3R$ subtypes highlight the different patterns of $IP_3R2$ expression (Fig. 1, *A–D*, *fourth column*). Representative fields of cells are shown in supplemental Fig. S2. The punctate distribution of $IP_3R2$ in unstimulated COS-7 cells is consistent with evidence that although all three $IP_3R$ subtypes can cluster when cells are stimulated (10, 11, 13), clustering of $IP_3R2$ appears to occur at resting levels of $IP_3$ (12).

**TABLE 1**

***D* and $M_f$ for $IP_3R$, RyR, SERCA, and EGFP-KDEL**

The results (means ± S.E. from *n* cells) show *D* and $M_f$ derived from experiments similar to those shown in Figs. 3 and 4 and supplemental Fig. S7. ND, not determined.

| | *D* | $M_f$ | *n* |
|---|---|---|---|
| | $\mu m^2/s$ | % | |
| $IP_3R1$ | 0.018 ± 0.001 | 84 ± 2 | 30 |
| $IP_3R2$ | 0.004 ± 0.001 | 47 ± 4 | 26 |
| $IP_3R3$ | 0.016 ± 0.002 | 80 ± 2 | 23 |
| RyR1 | 0.013 ± 0.003 | 76 ± 2 | 13 |
| SERCA1 | 0.024 ± 0.002 | 82 ± 1 | 22 |
| EGFP-KDEL | ND | 92 ± 4 | 17 |

Most cells express more than one $IP_3R$ subtype (1, 41), and the different subtypes assemble into both homo- and heterotetramers (39). COS-1 cells express $IP_3R3$ (~62%) and $IP_3R2$ (~37%) (42), and heterotetrameric assemblies of $IP_3R1$ and $IP_3R3$ have been detected when they are heterologously expressed in COS-7 cells (39). Co-assembly of transfected $IP_3R$ with native subunits is unlikely to distort our results because there is minimal association of endogenous and transfected $IP_3R$ (39). Because many native $IP_3R$ are likely to be hetero-oligomeric, we therefore examined the distribution of $IP_3R$ in cells cotransfected with equal amounts of plasmids encoding two $IP_3R$ subtypes. When EYFP-$IP_3R1$ was cotransfected with ECFP-$IP_3R3$, both were, as expected, uniformly distributed within the ER (Fig. 2*A*). Coexpression of EYFP-$IP_3R1$ with FLAG-$IP_3R2$ proved difficult. Most cells expressed only one $IP_3R$ subtype, and in the very rare cases where both were expressed, the distributions were ambiguous (data not shown). Coexpression of FLAG-$IP_3R2$ with ECFP-$IP_3R3$ resulted in a distribution that was indistinguishable from that of ECFP-$IP_3R3$, with no evidence of puncta (Fig. 2*B*). Others have shown that a splice variant of $IP_3R2$ ($IP_3R2_{m2}^{-}$) that lacks a functional $IP_3$-binding site fails to cluster, and its coexpression with either $IP_3R1$ or $IP_3R3$ prevents ATP from evoking their clustering (12). Collectively, these results demonstrate the complexity of the interactions within heterotetrameric $IP_3R$, but the most important point for the present work is that expressed $IP_3R2$ can assemble with $IP_3R3$ without perturbing the subcellular distribution of the latter. This provides persuasive evidence that the punctate distribution of $IP_3R2$ is unlikely to result from its misfolding. These results provide justification for using COS-7 cells to measure, for the first time, the relative mobilities of the three $IP_3R$ subtypes in exactly the same cellular environment.

*Differential Mobilities of $IP_3R$ Subtypes*—FRAP was used to measure the $M_f$ (mobile fraction) and $t_{½}$ (half-time for recovery of fluorescence), from which *D* (lateral diffusion coefficient) was calculated (see "Experimental Procedures"). Control experiments with fixed cells confirmed that there was no recovery of fluorescence within 5–6 min in the photobleached area in cells expressing EGFP-tagged $IP_3R1$ (supplemental Fig. S3). We note, however, not least because EYFP-tagged proteins are often used for both FRAP and FRET analyses, that there was substantial reversible bleaching of EYFP constructs (supplemental Fig. S4 and Table S1). In subsequent FRAP analyses, we avoided EYFP-tagged proteins.

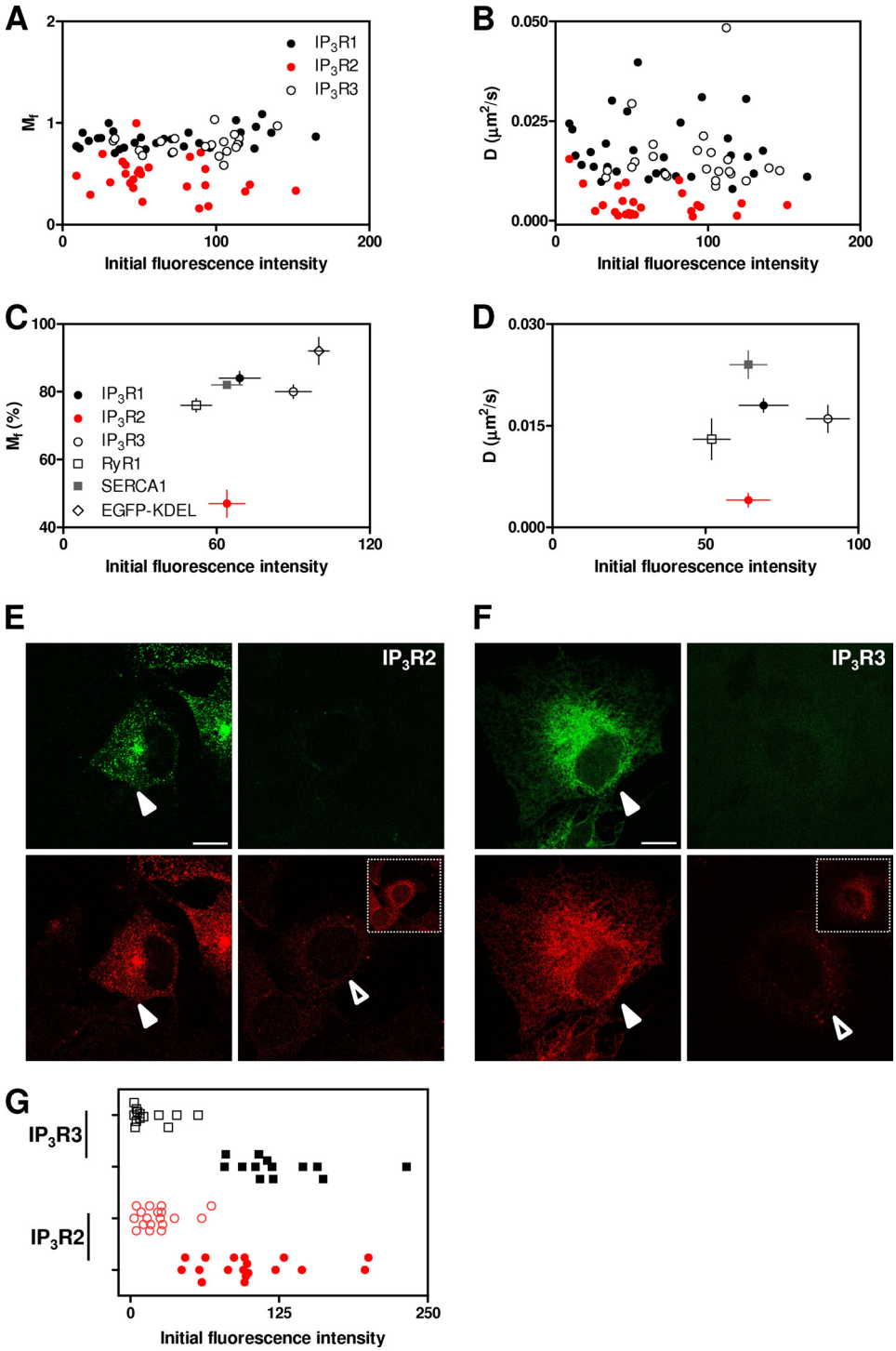


FIGURE 4. **Expression of EGFP-tagged $IP_3R$ subtypes does not perturb measurements of the mobile fraction or diffusion coefficient.** $M_f$ (*A*) and *D* (*B*) are shown for each cell expressing each $IP_3R$ subtype as a function of the background-corrected initial pre-bleach fluorescence intensity. Because each $IP_3R$ subtype has the same tag, the latter provides a measure of the relative expression level of each subtype. The results demonstrate considerable, but comparable, variation in the levels of expression of each EGFP-$IP_3R$ subtype and no relationship between the expression level and measured $M_f$ or *D*. The relationship between the average levels of expression for each $IP_3R$ subtype, RyR1, SERCA1, and EGFP-KDEL are shown for $M_f$ (*C*) and *D* (*D*). The results (*x* and *y coordinates*) are means ± S.E. for 13–30 cells. *E*, typical confocal images of COS-7 cells show fields that include cells transfected with EGFP-$IP_3R2$ and used for FRAP analyses (*left panels*, *closed arrowheads*) or non-transfected cells (*right panels*, *open arrowhead*). The *upper panels* show EGFP fluorescence (*green*), and the *lower panels* show immunostaining for $IP_3R2$ (*red*). The *inset* shows the same field imaged at higher laser intensity to show more clearly the immunostaining of endogenous $IP_3R2$. *F*, cells transfected with EGFP-$IP_3R3$ and immunostained for $IP_3R3$ are shown in the same format as described for *E*. *Scale bars* (*E* and *F*) = 10 $\mu$m. *G*, from fields similar to those shown in *E* and *F*, cells expressing EGFP-$IP_3R$ at levels suitable for FRAP analyses were identified and compared with neighboring cells lacking EGFP-$IP_3R$. The levels of immunostaining in perinuclear ROI were then quantified for the two cell populations for each $IP_3R$ subtype. The results (means ± S.E. for 13–18 cells) show immunostaining for each non-transfected (*open symbols*) and transfected (*closed symbols*) cell.

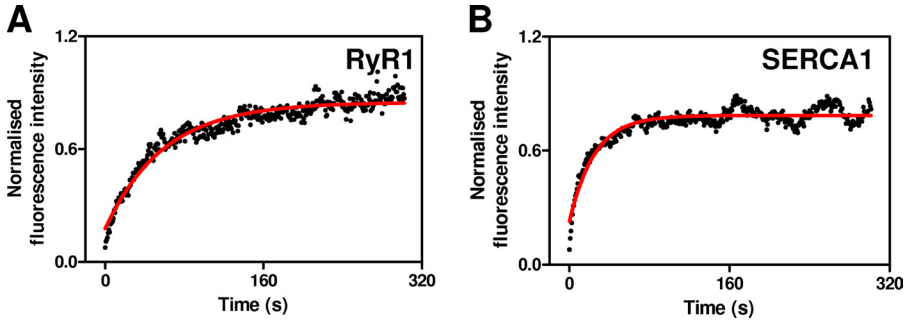


FIGURE 5. **Mobilities of EGFP-RyR1 and SERCA1-EGFP.** *A* and *B*, normalized fluorescence intensities from the ROI after photobleaching as a function of time for EGFP-RyR1 and SERCA1-EGFP, respectively. *Red lines* show the monoexponential curve fits to the recovery phase. The results show typical examples of the results summarized in Table 1.

Fig. 3*A* shows typical images during a FRAP experiment with EGFP-$IP_3R1$, highlighting the three regions selected for detailed analysis: the ROI (the 2.5-$\mu$m diameter bleached area), the entire cell, and a background area lying outside the cell. In all experiments, the ROI was selected to lie in the perinuclear region, at a distance >2 $\mu$m from the nucleus or the plasma membrane. Fig. 3*B* shows time courses of the raw fluorescence intensities from each of these three regions for typical cells expressing EGFP-tagged $IP_3R1$, $IP_3R2$, or $IP_3R3$. The time courses of the recovery of fluorescence within the bleached area (ROI), corrected for both background fluorescence and the decrease in overall fluorescence of the cell due to bleaching of the ROI and imaging (see "Experimental Procedures"), were each fitted to single exponential equations (Fig. 3*C*), from which $M_f$ and $D$ were calculated (Fig. 3, *D* and *E*). An alternative analysis (36, 43), derived via a theoretical examination of FRAP kinetics, provided results consistent with the conclusions derived from our simpler monoexponential curve fitting, although with slightly increased values for both $M_f$ and $D$ for all proteins (supplemental Fig. S5).

The results demonstrate that most $IP_3R1$ and $IP_3R3$ are mobile ($M_f = 84 \pm 2$ and $80 \pm 2\%$, respectively) and with indistinguishable diffusion coefficients ($D = 0.018 \pm 0.001$ and $0.016 \pm 0.002$ $\mu m^2/s$, respectively) (Table 1). Comparable measurements of $IP_3R2$ revealed a smaller mobile fraction ($47 \pm 4\%$) and a lesser diffusion coefficient ($0.004 \pm 0.001$ $\mu m^2/s$) (Table 1).

*FRAP Measurements without Perturbing $IP_3R$ Mobility*—An inevitable concern with FRAP analyses is that heterologous expression of a fluorescent protein might overwhelm the cellular machinery that normally determines the distribution and mobility of the native protein. To minimize such problems, we selected cells with the lowest acceptable levels of expression of EGFP-$IP_3R$ compatible with the FRAP analyses. By performing FRAP experiments in parallel under identical conditions for each $IP_3R$ subtype, we could compare the levels of expression of each EGFP-tagged $IP_3R$ subtype in each cell with the measured $M_f$ and $D$. The results demonstrate, first, that the expression levels of the three $IP_3R$ subtypes were comparable and, second, that for each there was no correlation across an almost 15-fold range of expression level between either $M_f$ or $D$ and the amount of EGFP-$IP_3R$ expressed (Fig. 4, *A*–*D*).

To allow direct comparison of the endogenous levels of expression of $IP_3R$ with those prevailing after expression of EGFP-$IP_3R$, cells prepared for FRAP experiments were immunostained with antibodies that recognize $IP_3R2$ or $IP_3R3$, the predominant endogenous $IP_3R$ subtypes in COS cells (42). The antibodies selectively recognize both endogenous and tagged $IP_3R$ subtypes. Cells in which the expression of EGFP-$IP_3R2$ (or EGFP-$IP_3R3$) matched our criteria for analysis by FRAP were compared with those in which there was no detectable expression of EGFP, and for each category, we compared the cell immunostaining for $IP_3R2$ (or $IP_3R3$) in a perinuclear ROI. The results show that in the cells used for FRAP, background-corrected immunofluorescence (in arbitrary units of fluorescence) was $101 \pm 10$ ($n = 18$) for transfected $IP_3R2$ and $125 \pm 11$ ($n = 13$) for transfected $IP_3R3$, compared with $23 \pm 4$ and $16 \pm 5$ in non-transfected cells, respectively (Fig. 4, *E*–*G*). These results establish that in the FRAP analyses, the average levels of $IP_3R2$ and $IP_3R3$ expression were increased by ~4- and 8-fold, respectively. We are unaware of any previous attempt to compare quantitatively the levels of overexpression required to perform FRAP analyses. Although the average levels of $IP_3R$ expression were increased in the cells used for FRAP analyses, there was considerable variability between individual cells (Fig. 4*G*). It is noteworthy that $IP_3R$ expression levels in native cells with the highest levels of expression and in transfected cells with the lowest levels were similar (and considerably overlapped for $IP_3R2$) (Fig. 4*G*). These results, together with our demonstration that there is no correlation across an ~15-fold difference in expression level between $IP_3R$ expression and $M_f$ or $D$ (Fig. 4, *A* and *B*), provide evidence that under the conditions of our experiments, FRAP is likely to report faithfully the motility of the endogenous $IP_3R$ population.

*Comparison of the Mobility of $IP_3R$ with That of Other ER Proteins*—In parallel FRAP analysis of EGFP-RyR1, which is likely to have transmembrane structures similar to $IP_3R$ (44) and which is also expressed in the ER, both $D$ ($0.013 \pm 0.003$ $\mu m^2/s$) and $M_f$ ($76 \pm 2\%$) (Fig. 5*A* and Table 1) were similar to those determined for $IP_3R1$ and $IP_3R3$. SERCA1-EGFP, an ER membrane protein with fewer transmembrane domains than a tetrameric $IP_3R$ (10 *versus* 24), had the same $M_f$ ($82 \pm 1\%$) as $IP_3R1$ and $IP_3R3$ but a slightly increased $D$ ($0.024 \pm 0.002$ $\mu m^2/s$) (Fig. 5*B* and Table 1). The difference in $D$ between $IP_3R$ and SERCA1, which is similar to that reported for SERCA2a and $IP_3R1$ (23), is rather larger than expected for two freely diffusing proteins for which mobility is deter-

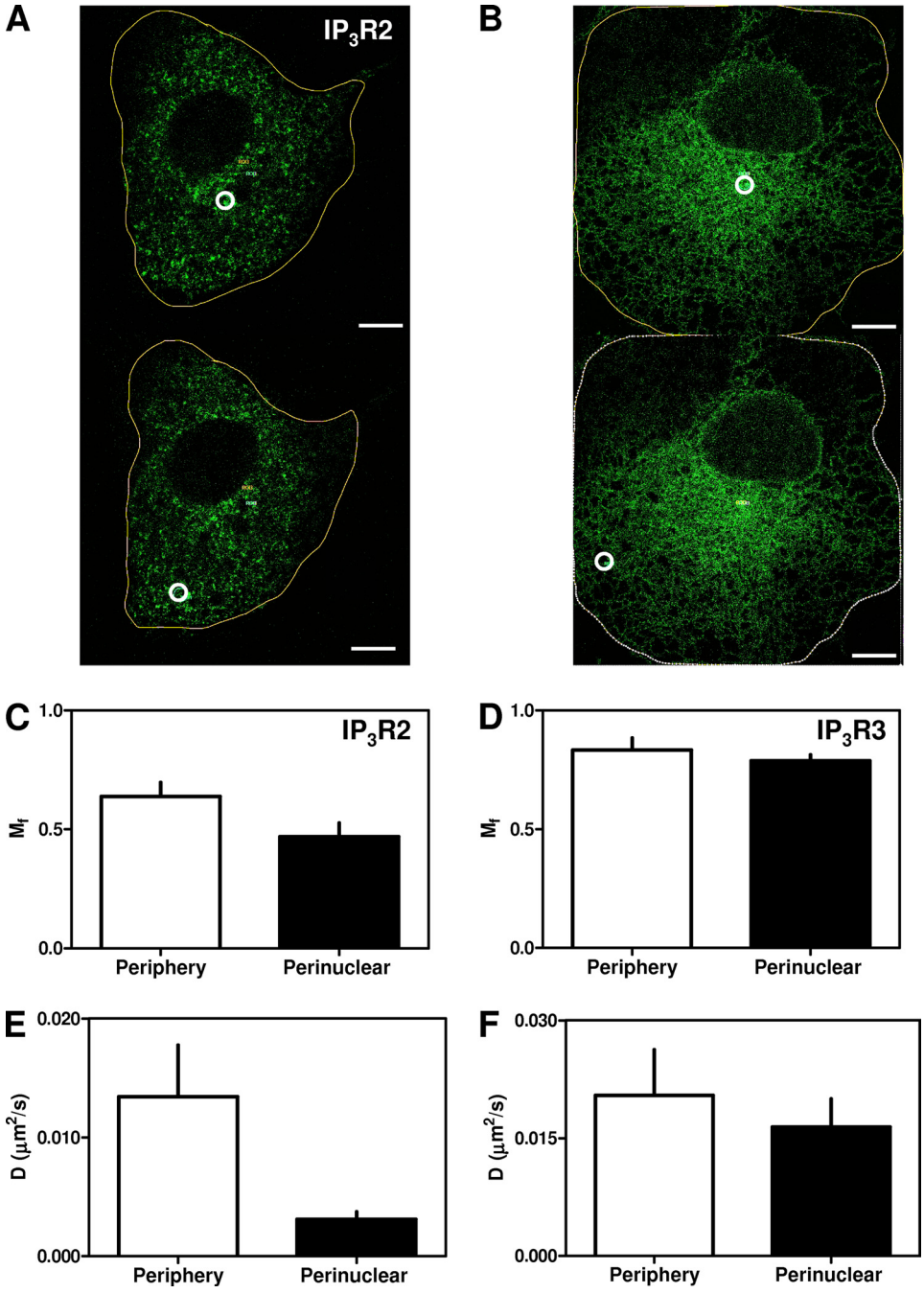


FIGURE 6. **Differential mobility of $IP_3R2$ in different subcellular regions.** Typical FRAP experiments are shown for EGFP-$IP_3R2$ (*A*) and EGFP-$IP_3R3$ (*B*), with ROI (*white circles*) chosen to capture $IP_3R$ within the perinuclear (*upper panels*) or peripheral (*lower panels*) regions of the cell. Images are shown after recovery periods of at least 300 s. *Scale bars* = 10 $\mu$m. The results are typical of recordings from 10–15 cells from three independent transfections. Summary results (means ± S.E., $n$ = 10–15) are shown for $M_f$ (*C* and *D*) and $D$ (*E* and *F*) determined for each $IP_3R$ subtype in the cell periphery (*open bars*) or perinuclear region (*closed bars*).

mined solely by the number of transmembrane domains (supplemental Fig. S6). There are several possible explanations for the disparity. SERCA may move by both diffusion and active transport and thereby provide an inappropriate benchmark for comparison with proteins moving only by diffusion. The mobility of $IP_3R$ may be hampered by association with cytoskeletal structures (19, 20, 23). Protein 4.1, for example, selectively associates with $IP_3R1$ (20, 45), and disrupting actin filaments increases the diffusion of $IP_3R1$ in Purkinje cells (23) and hippocampal neurons (20). Disruption of microtubules has also been reported to increase the mobility of $IP_3R1$ (20) and $IP_3R3$ (19). Alternatively, assembly of $IP_3R1$ or $IP_3R3$ into small clusters of approximately seven $IP_3R$ would be sufficient to account for the lesser $D$ relative to SERCA (see legend to supplemental Fig. S6 for further details). Our measurements of $D$ (Table 1), whether they reflect movement of single or clustered $IP_3R$, indicate that $IP_3R1$ or $IP_3R3$ can move ~1 $\mu$m within the two dimensions of a lipid membrane in ~10 s (mean displacement, $|r| = \sqrt{4Dt}$) (46).

An elegant functional analysis of SH-SY5Y neuroblastoma cells, which express predominantly $IP_3R1$ (42), assumed that movement of the sites from which the smallest $Ca^{2+}$ release events originate reflected movement of single $IP_3R$ and thereby estimated $D$ for functional $IP_3R1$ to be between 0.003 $\mu m^2/s$ (47) and 0.012 $\mu m^2/s$ (18). It is unclear, however, whether this estimate, which suggests that $IP_3R1$ diffuses considerably more slowly than suggested by our FRAP analysis (Table 1), reflects the immobility of a site to which freely moving $IP_3R$ transiently attach or the mobility of the $IP_3R$ themselves. In addition, it is not clear whether the $Ca^{2+}$ signals arise from an isolated $IP_3R$ or a single active $IP_3R$ within a larger cluster. We note, too, that there is substantial variation in $D$ determined for $IP_3R1$ in different cells (0.004–0.26 $\mu m^2/s$) (supplemental Table S2).

EGFP expressed within the lumen of the ER (EGFP-KDEL) diffused too quickly for $D$ to be measured, but it was possible to measure $M_f$ (supplemental Fig. S7). $M_f$ determined for this luminal protein (92 ± 4%) was similar to that determined for most of the membrane proteins ($IP_3R1$, $IP_3R3$, and SERCA1). Only RyR1 (76 ± 2%) and $IP_3R2$ (47 ± 4%) had significantly smaller $M_f$ (Table 1). The consistent $M_f$ between several ER membrane proteins and a luminal protein suggests that the immobile fraction probably arises from discontinuities within the ER rather than immobile proteins within a continuous organelle. We conclude that the majority (and perhaps all) of $IP_3R1$ and $IP_3R3$ move freely within the membranes of the ER and with similar diffusion coefficients. However, $IP_3R2$ is different: it has a significantly smaller $D$ and $M_f$ (Table 1).

*Subcellular Heterogeneity in the Motility of $IP_3R2$*—$D$ for $IP_3R2$, which has not to our knowledge been reported previously, is significantly lower than for $IP_3R1$ or $IP_3R3$ (Table 1). If this lesser $D$ were due only to clustering, it would require the clusters to include >900 $IP_3R2$ (supplemental Fig. S6). This is implausible, given the number of puncta and likely density of $IP_3R$ (probably $<10^5$ $IP_3R$/cell) (48). Therefore, the slower diffusion of $IP_3R2$ relative to $IP_3R1$ and $IP_3R3$ is not a direct consequence of the propensity of $IP_3R2$ to cluster. This suggests that clustering and reduced mobility are independent properties of $IP_3R2$. Further studies are required to establish whether these distinctive behaviors of $IP_3R2$ are expressed in all cell types or whether they require additional endogenous proteins that may be selectively expressed in only some cells, such as COS-7 cells.

We used FRAP to examine the mobility of $IP_3R2$ and $IP_3R3$ in different subcellular regions (Fig. 6, *A* and *B*). $IP_3R2$ receptors adjacent (~2 $\mu m$) to the plasma membrane were considerably more mobile ($M_f = 64 \pm 6\%$ and $D = 0.013 \pm 0.004$ $\mu m^2/s$, $n = 15$) than those in the perinuclear region ($M_f = 47 \pm 6\%$ and $D = 0.003 \pm 0.001$ $\mu m^2/s$, $n = 15$) (Fig. 6, *C* and *E*). By contrast, $IP_3R3$ (the other major endogenous $IP_3R$ subtype in COS cells) had similar properties in the perinuclear ($M_f = 79 \pm 2\%$ and $D = 0.016 \pm 0.004$ $\mu m^2/s$, $n = 10$) (a subset of the data presented in Table 1) and peripheral ($M_f = 83 \pm 5\%$ and $D = 0.020 \pm 0.006$ $\mu m^2/s$, $n = 10$) regions (Fig. 6, *D* and *F*). These results establish that both the diffusion and mobile fraction of $IP_3R2$ differ between subcellular regions.

*Conclusions*—Using FRAP methods that seem unlikely to perturb the mobility of $IP_3R$ (Fig. 4), we have compared the mobility of all three mammalian $IP_3R$ subtypes in the same cellular background. We conclude that $IP_3R1$ and $IP_3R3$ move freely and with similar diffusion coefficients within ER membranes that seem largely, although not entirely, continuous throughout the cell (Figs. 3 and 5 and Table 1). $IP_3R2$ is different in that it forms puncta (Fig. 1), and its mobility differs between subcellular regions (Fig. 6). In perinuclear regions, 53% of $IP_3R2$ diffuse slowly, and the remainder are immobile, whereas close to the plasma membrane, 36% are immobile, and the rest diffuse at rates similar to those of the other $IP_3R$ subtypes. We conclude that $IP_3R1$ and $IP_3R3$ diffuse freely within a largely continuous ER, but $IP_3R2$ is more heterogeneously distributed and less mobile, and its mobility differs between regions of the cell. The latter may be important for initiation of $IP_3$-evoked $Ca^{2+}$ release because $IP_3R2$ is the most sensitive of the $IP_3R$ subtypes to $IP_3$ (12, 30) and perhaps thereby the most likely to initiate $Ca^{2+}$ signals.

*Acknowledgments—We thank Drs. S. Dedos, A. Parker, G. Meur, F. Wolfram, and Z. Ding (all originally in the Department of Pharmacology, University of Cambridge) for providing $IP_3R$ and RyR plasmids or helping with their preparation. The plasmid for SERCA1-EGFP was provided by Dr. Malcolm East. EGFP-KDEL was provided by Dr. Peter Haggie. The rabbit anti-$IP_3R2$ antibody was provided by Dr. David Yule. We thank Drs. J. Skepper and G. Hammond (University of Cambridge) for help with confocal microscopy and FRAP, respectively.*

## REFERENCES

1. Taylor, C. W., Genazzani, A. A., and Morris, S. A. (1999) *Cell Calcium* **26,** 237–251
2. Foskett, J. K., White, C., Cheung, K. H., and Mak, D. O. (2007) *Physiol. Rev.* **87,** 593–658
3. Marchant, J. S., and Taylor, C. W. (1997) *Curr. Biol.* **7,** 510–518
4. Mak, D. O., McBride, S., and Foskett, J. K. (1998) *Proc. Natl. Acad. Sci. U.S.A.* **95,** 15821–15825
5. Bootman, M. D., and Berridge, M. J. (1995) *Cell* **83,** 675–678
6. Marchant, J., Callamaras, N., and Parker, I. (1999) *EMBO J.* **18,** 5285–5299
7. Smith, I. F., and Parker, I. (2009) *Proc. Natl. Acad. Sci. U.S.A.* **106,** 6404–6409
8. Berridge, M. J., Lipp, P., and Bootman, M. D. (2000) *Nat. Rev. Mol. Cell Biol.* **1,** 11–21
9. Bootman, M. D., and Berridge, M. J. (1996) *Curr. Biol.* **6,** 855–865
10. Wilson, B. S., Pfeiffer, J. R., Smith, A. J., Oliver, J. M., Oberdorf, J. A., and Wojcikiewicz, R. J. H. (1998) *Mol. Biol. Cell* **9,** 1465–1478
11. Chalmers, M., Schell, M. J., and Thorn, P. (2006) *Biochem. J.* **394,** 57–66
12. Iwai, M., Tateishi, Y., Hattori, M., Mizutani, A., Nakamura, T., Futatsugi, A., Inoue, T., Furuichi, T., Michikawa, T., and Mikoshiba, K. (2005) *J. Biol. Chem.* **280,** 10305–10317
13. Tateishi, Y., Hattori, M., Nakayama, T., Iwai, M., Bannai, H., Nakamura, T., Michikawa, T., Inoue, T., and Mikoshiba, K. (2005) *J. Biol. Chem.* **280,** 6816–6822
14. Mak, D. O., and Foskett, J. K. (1997) *J. Gen. Physiol.* **109,** 571–587
15. Mak, D. O., McBride, S., Raghuram, V., Yue, Y., Joseph, S. K., and Foskett, J. K. (2000) *J. Gen. Physiol.* **115,** 241–256
16. Rahman, T., and Taylor, C. W. (2009) *Channels* **3,** 226–232
17. Taufiq-Ur-Rahman, Skupin, A., Falcke, M., and Taylor, C. W. (2009) *Nature* **458,** 655–659
18. Smith, I. F., Wiltgen, S. M., Shuai, J., and Parker, I. (2009) *Sci. Signal.* **2,** ra77
19. Ferreri-Jacobia, M., Mak, D. O., and Foskett, J. K. (2005) *J. Biol. Chem.* **280,** 3824–3831
20. Fukatsu, K., Bannai, H., Zhang, S., Nakamura, H., Inoue, T., and Mikoshiba, K. (2004) *J. Biol. Chem.* **279,** 48976–48982

21. Gibson, C. J., and Ehrlich, B. E. (2008) *Cell Calcium* **43,** 228–235
22. Cruttwell, C., Bernard, J., Hilly, M., Nicolas, V., Tunwell, R. E., and Mauger, J. P. (2005) *Biol. Cell* **97,** 699–707
23. Fukatsu, K., Bannai, H., Inoue, T., and Mikoshiba, K. (2010) *J. Neurochem.* **114,** 1720–1733
24. Mignery, G. A., Newton, C. L., Archer, B. T., 3rd, and Südhof, T. C. (1990) *J. Biol. Chem.* **265,** 12679–12685
25. Cardy, T. J., and Taylor, C. W. (1998) *Biochem. J.* **334,** 447–455
26. Blondel, O., Takeda, J., Janssen, H., Seino, S., and Bell, G. I. (1993) *J. Biol. Chem.* **268,** 11356–11363
27. Parker, A. K., Gergely, F. V., and Taylor, C. W. (2004) *J. Biol. Chem.* **279,** 23797–23805
28. Pantazaka, E., and Taylor, C. W. (2010) *Biochem. J.* **425,** 61–69
29. Wolfram, F., Morris, E., and Taylor, C. W. (2010) *Biochem. J.* **428,** 483–489
30. Tovey, S. C., Dedos, S. G., Rahman, T., Taylor, E. J., Pantazaka, E., and Taylor, C. W. (2010) *J. Biol. Chem.* **285,** 12979–12989
31. Newton, T., Black, J. P., Butler, J., Lee, A. G., Chad, J., and East, J. M. (2003) *Biochem. J.* **371,** 775–782
32. Dayel, M. J., Hom, E. F., and Verkman, A. S. (1999) *Biophys. J.* **76,** 2843–2851
33. Meur, G., Parker, A. K., Gergely, F. V., and Taylor, C. W. (2007) *J. Biol. Chem.* **282,** 23096–23103
34. Betzenhauser, M. J., Fike, J. L., Wagner, L. E., 2nd, and Yule, D. I. (2009) *J. Biol. Chem.* **284,** 25116–25125
35. Rabut, G., and Ellenberg, J. (2004) in *Live Cell Imaging: A Laboratory Manual* (Goldman, R. D., and Spector, D. L., eds) pp. 101–126, Cold Spring Harbor Laboratory Press, Woodbury, NY
36. Axelrod, D., Koppel, D. E., Schlessinger, J., Elson, E., and Webb, W. W. (1976) *Biophys. J.* **16,** 1055–1069
37. Laflamme, K., Domingue, O., Guillemette, B. I., and Guillemette, G. (2002) *J. Cell. Biochem.* **85,** 219–228
38. Ramos-Franco, J., Bare, D., Caenepeel, S., Nani, A., Fill, M., and Mignery, G. (2000) *Biophys. J.* **79,** 1388–1399
39. Joseph, S. K., Bokkala, S., Boehning, D., and Zeigler, S. (2000) *J. Biol. Chem.* **275,** 16084–16090
40. Sheppard, C. A., Simpson, P. B., Sharp, A. H., Nucifora, F. C., Ross, C. A., Lange, G. D., and Russell, J. T. (1997) *J. Neurochem.* **68,** 2317–2327
41. Vermassen, E., Parys, J. B., and Mauger, J. P. (2004) *Biol. Cell* **96,** 3–17
42. Wojcikiewicz, R. J. H. (1995) *J. Biol. Chem.* **270,** 11678–11683
43. Kwon, G., Axelrod, D., and Neubig, R. R. (1994) *Cell. Signal.* **6,** 663–679
44. Samso, M., Wagenknecht, T., and Allen, P. D. (2005) *Nat. Struct. Mol. Biol.* **6,** 539–544
45. Fukatsu, K., Bannai, H., Inoue, T., and Mikoshiba, K. (2006) *Biochem. Biophys. Res. Commun.* **342,** 573–576
46. Berg, H. C. (1983) *Random Walks in Biology*, Princeton University Press, Princeton, NJ
47. Wiltgen, S. M., Smith, I. F., and Parker, I. (2010) *Biophys. J.* **99,** 437–446
48. Tovey, S. C., Dedos, S. G., Taylor, E. J., Church, J. E., and Taylor, C. W. (2008) *J. Cell Biol.* **183,** 297–311